INSTITUTE OF PHYSICS PUBLISHING JOURNAL OF OPTICS A: PURE AND APPLIED OPTICS

J. Opt. A: Pure Appl. Opt. **8** (2006) 867–877 doi:10.1088/1464-4258/8/10/008

General construction and connections of vector propagation invariant optical fields: TE and TM modes and polarization states

Karen Volke-Sepulveda and Eugenio Ley-Koo

Instituto de Física UNAM, Apartado Postal 20-364, 01000 México, DF, Mexico

E-mail: karen@fisica.unam.mx and eleykoo@fisica.unam.mx

Received 8 June 2006, accepted for publication 31 July 2006
Published 18 August 2006
Online at stacks.iop.org/JOptA/8/867

Abstract
Rigorous solutions of the Maxwell equations describing propagation invariant optical fields are presented in general; the elements for their specific applications to the Bessel, Mathieu and Weber families are also provided. Electric and magnetic transverse modes, and several polarization state solutions, are constructed; the connections between them are explicitly established. Their respective energy densities and Poynting vectors are also evaluated, in order to exhibit their propagation invariant nature. The experience with Bessel beams allows us to recognize that vector modes exhibit new and important features compared with the corresponding scalar fields; the results of this work constitute a first step towards the analysis of the dynamical properties of vector Mathieu and Weber beams.

Keywords: non-diffracting beams, polarization, propagation invariant optical fields

(Some figures in this article are in colour only in the electronic version)

1. Introduction

It will soon be twenty years since the concept of non-diffracting beams was introduced by Durnin and co-workers in their study of the scalar Bessel beam [1, 2]. Of course, the plane wave is the most elementary example of a non-diffracting beam or propagation invariant optical field (PIOF), characterized by a transverse intensity profile that remains unchanged on propagation over arbitrarily extended distances. In general, any solution of the wave equation of the separable form $\Psi(\mathbf{r}, t) = \exp[\mathrm{i}(k_z z \pm \omega t)]\psi(q_1, q_2)$, where (q_1, q_2) are generalized transverse cylindrical coordinates, represents a scalar PIOF. Apart from the plane waves in Cartesian coordinates (x, y, z) and Bessel beams in circular cylindrical coordinates (ρ, φ, z), other scalar PIOFs have been investigated in recent years: Mathieu beams in elliptical cylindrical coordinates (u, v, z) [3], and parabolic non-diffracting beams or Weber PIOFs in parabolic cylindrical coordinates (ξ, η, z) [4, 5]. Each set of plane, Bessel, Mathieu and Weber waves is a complete and orthonormal basis, with separable transverse components $\psi(q_1, q_2) = Q_1(q_1)Q_2(q_2)$ covering the entire $(q_1, q_2, z = z_0)$ plane. Any arbitrary optical field can be expanded as superpositions of the alternative PIOF bases, underlining the latter's special and important role. For instance, the Gauss modulated beams of the Bessel, Mathieu and Weber types with a finite transverse extent, introduced in [6–8], can be constructed as superpositions of PIOFs.

On the other hand, rigorous vector solutions of the Maxwell equations are well known for plane waves, but they have been analysed for Bessel beams only in the last decade [9–12]. A very recent publication introduced vector Helmholtz–Gauss beams [13], which correspond to vector versions of the finite paraxial approximation to PIOFs, and they become PIOFs in the limit of the Gaussian beam waist size infinitely large. Most of the above analyses have been restricted to transverse electric (TE) and transverse magnetic (TM) modes. Reference [12] includes the analysis of alternative polarization states. Experimental approximations of both scalar [11, 14] and vector [15] high-order Bessel beams have been implemented in free space, allowing us to establish that different polarization states possess different angular momentum properties [11, 15, 16]. Therefore, a full vector

description of PIOFs is important in order to characterize the polarization states, and also as a first and fundamental step towards the identification and study of the dynamical properties of the vector optical fields.

In this paper, several solutions of the Maxwell equations are constructed, establishing the connections between them as well as their PIOF character. In section 2, the vector solutions of the Maxwell equations are obtained as the successive curls of $\hat{\mathbf{k}}\Phi(\mathbf{r},t)$ and $(\hat{\mathbf{e}}_x \pm \mathrm{i}\hat{\mathbf{e}}_y)\Psi(\mathbf{r},t)$, where Φ and Ψ are scalar PIOFs. In the first case, the resulting fields are identified as TE and TM modes, while in the second case they correspond to left- and right-handed 'circularly polarized' states; appropriate combinations of such modes or states are also identified as alternative polarization states. In section 3, the general connections between the 'circularly polarized' states associated with the respective Φ and Ψ PIOFs are explicitly established. In section 4, the energy density and Poynting vector of the optical fields are evaluated; their general and explicit expressions, in terms of Φ (Ψ) and their transverse derivatives, exhibit their propagation invariant property. Appendix A contains the explicit relationships between the Cartesian $(\hat{\mathbf{e}}_x, \hat{\mathbf{e}}_y, \hat{\mathbf{e}}_z)$ and 'circularly polarized' $(\hat{\mathbf{e}}_+, \hat{\mathbf{e}}_-, \hat{\mathbf{e}}_z)$ vector bases, and the corresponding components of vectors and their operations. Appendix B provides the connections between the Cartesian and circular, elliptical and parabolic cylindrical coordinates, scale factors and unit vectors, in order to implement the respective operations for the specific cases of Bessel, Mathieu and Weber optical fields.

2. Construction of general vector modes of PIOFs

Vector propagation invariant optical fields, identified as solutions of the Maxwell equations, correspond to solenoidal electric and magnetic fields which are the curls of each other

$$\nabla \times \mathbf{H}(\mathbf{r}) = -\mathrm{i}\omega\epsilon\mathbf{E}(\mathbf{r}), \tag{1}$$

$$\nabla \times \mathbf{E}(\mathbf{r}) = \mathrm{i}\omega\mu\mathbf{H}(\mathbf{r}), \tag{2}$$

as required by the Maxwell and Faraday laws, respectively. We have assumed harmonic time dependence of the form $\exp\{-\mathrm{i}\omega t\}$. The decoupling of equations (1) and (2), by taking their respective curls, leads to the Helmholtz equation for each field

$$\left(\nabla^2 + \frac{\omega^2}{c^2}\right)\left\{\begin{matrix}\mathbf{E}\\ \mathbf{H}\end{matrix}\right\} = 0, \tag{3}$$

where $c = 1/\sqrt{\epsilon\mu}$, and $\omega^2/c^2 = k^2 = k_t^2 + k_z^2$, incorporating the distinction between the transverse (k_t) and longitudinal (k_z) components of the propagation vector.

The scalar PIOFs are also solutions of the Helmholtz equation and the starting elements to construct the vector PIOF solutions of (1)–(3). The basis for such a construction is the following theorem: for a given a solution $\Psi(\mathbf{r})$ of the Helmholtz equation, its Cartesian derivatives $\partial\Psi/\partial x_i$, $x_i = x, y, z$, are also solutions of the same equation. In fact, we follow Stratton [17] to introduce the set of vector fields:

$$\mathbf{M}(\mathbf{r}) = \nabla \times \left[\hat{\mathbf{a}}\Psi(\mathbf{r})\right]; \tag{4}$$

$$\mathbf{N}(\mathbf{r}) = \frac{1}{k}\nabla \times \mathbf{M} = \frac{1}{k}\nabla\left[\nabla \cdot \left(\hat{\mathbf{a}}\Psi(\mathbf{r})\right)\right] + \hat{\mathbf{a}}k\Psi(\mathbf{r}), \tag{5}$$

where $\hat{\mathbf{a}}$ is an arbitrary constant unit vector. Both fields are obviously solenoidal; they form a group under the curl operation, since it is straightforward to prove that

$$\frac{1}{k}\nabla \times \mathbf{N} = \mathbf{M}, \tag{6}$$

and also satisfy the Helmholtz equation.

Consequently, PIOF vector solutions of (1)–(3) can be written as linear superpositions of the $\mathbf{M}$ and $\mathbf{N}$ basis as

$$\mathbf{E}_s(\mathbf{r}) = c_s\mathbf{M}_s(\mathbf{r}) + d_s\mathbf{N}_s(\mathbf{r}), \tag{7}$$

$$\mathbf{H}_s(\mathbf{r}) = -\frac{\mathrm{i}k}{\omega\mu}\left[c_s\mathbf{N}_s(\mathbf{r}) + d_s\mathbf{M}_s(\mathbf{r})\right], \tag{8}$$

for each selection of unit vector $\hat{\mathbf{a}}$ and scalar PIOF

$$\Psi_s(\mathbf{r},t) = Q_1(q_1)Q_2(q_2)\exp\left\{\mathrm{i}\left(k_z z - \omega t\right)\right\}. \tag{9}$$

Here s is a generic label counting the successive values of the separation constant in the solutions of the transverse Helmholtz equation. In the case of Bessel beams, it corresponds to the eigenvalue of the z-component of the orbital angular momentum [11, 16]; for Mathieu beams, it is related to the scalar product $\mathbf{l}_1 \cdot \mathbf{l}_2$ of the orbital angular momenta with respect to the position of the foci defining the elliptical coordinates; and for Weber beams, it is connected with the magnitude of the Runge–Lenz vector $\nabla_\perp \times \mathbf{l}$, involving the cross product of the transverse Nabla and angular momentum operators [18]. The respective transverse functions correspond to the radial and angular Bessel–Fourier, Mathieu and Weber functions with common values s of the separation constants.

In the following subsections the vector fields $\mathbf{M}$ and $\mathbf{N}$ are generated for the selections: (1) $\hat{\mathbf{a}} = \hat{\mathbf{e}}_z$ and a scalar PIOF Φ_s, corresponding to transverse TE and TM modes, and (2) $\hat{\mathbf{a}} = \hat{\mathbf{e}}_\pm$ and a scalar PIOF Ψ_s, leading to left- and right-handed 'circular polarization' states. Appropriate combinations in (7) are also constructed and identified as alternative polarization states. Extensive use is made of the formulae in the appendices in order to represent the vector PIOFs in general and in the specific vector bases. Illustrative graphical representations of some of the vector PIOFs are shown as well.

2.1. *Transverse modes and some of their superposition polarization states*

For the selection of the unit vector $\hat{\mathbf{a}}$ in the longitudinal direction and the scalar space PIOF $\Phi_s(\mathbf{r}) = \phi_s(\boldsymbol{\rho})\exp(\mathrm{i}k_z z)$, equations (4) and (5) for the basis vector fields take the explicit forms

$$\begin{aligned}\mathbf{M}_s(\mathbf{r}) &= \left[\hat{\mathbf{e}}_x\frac{\partial}{\partial y} - \hat{\mathbf{e}}_y\frac{\partial}{\partial x}\right]\phi_s(\boldsymbol{\rho})\exp\left\{\mathrm{i}k_z z\right\}\\ &= \left[\hat{\mathbf{e}}_1\frac{1}{h_2}\frac{\partial}{\partial q_2} - \hat{\mathbf{e}}_2\frac{1}{h_1}\frac{\partial}{\partial q_1}\right]\phi_s(q_1,q_2)\exp\left\{\mathrm{i}k_z z\right\};\end{aligned} \tag{10}$$

$$\mathbf{N}_s(\mathbf{r}) = \frac{1}{k}\left[\mathrm{i}k_z\nabla_\perp + k_t^2\hat{\mathbf{e}}_z\right]\phi_s(q_1,q_2)\exp\left\{\mathrm{i}k_z z\right\} \tag{11}$$

where $h_i = h_i(q_1,q_2)$, with $i = 1, 2$, denote the respective scale factors for the curvilinear coordinates (see appendix B). Notice that while the vector $\mathbf{M}_s$ has two components in the transverse plane, the vector $\mathbf{N}_s$ has three components, two in the plane and one along the propagation axis. Since their

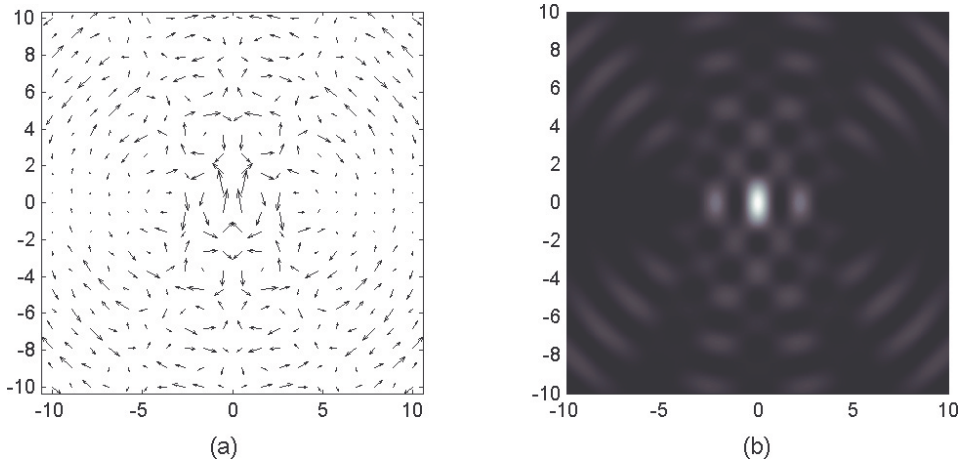

Figure 1. (a) Instant vector diagram ($t = 0$) of the electric field for a TE mode associated with the even-type Mathieu scalar PIOF $Je_3(u)ce_3(v)$ and focal semi-axis $f = 5\lambda$. (b) Transverse intensity distribution of the optical field. The ratio between the transverse and axial components of the wave vector corresponds to $k_t/k_z = 0.25$. Length scales are in units of λ.

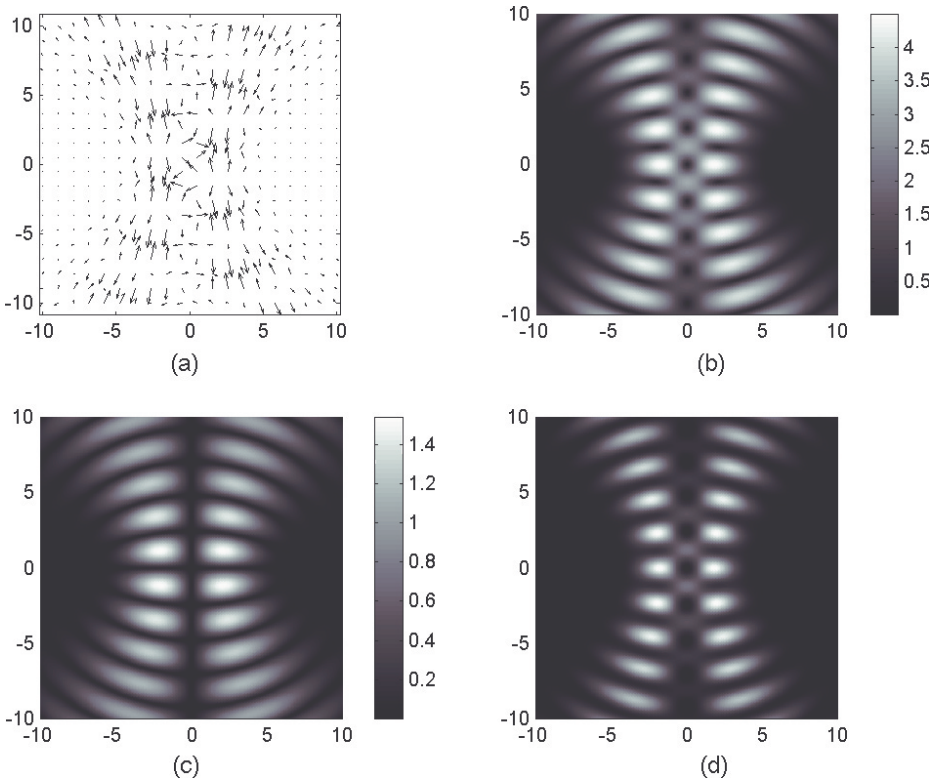

Figure 2. (a) Instant vector diagram ($t = 0$) and (b) magnitude of the transverse component of electric field for a TM mode associated with the odd-type Mathieu scalar PIOF $Jo_2(u)se_2(v)$, $f = 6.25\lambda$ and $k_t/k_z = 0.25$. (c) Magnitude of the axial component of the field. The colour bars illustrate the relative magnitudes between transverse and axial components. (d) Total intensity distribution at a given z plane. Length scales in units of λ.

respective transverse components are associated with the curl and transverse gradient of the scalar PIOF, both vectors are perpendicular to each other.

The choice $c_s = 1$ and $d_s = 0$ in (7) and (8) leads to the identification of the electric and magnetic fields of the TE mode

$$\mathbf{E}_s^{\mathrm{TE}}(\mathbf{r}) = \mathbf{M}_s(\mathbf{r}), \tag{12}$$

$$\mathbf{H}_s^{\mathrm{TE}}(\mathbf{r}) = -\frac{\mathrm{i}k}{\omega\mu}\mathbf{N}_s(\mathbf{r}). \tag{13}$$

The complementary choice of $c_s = 0$ and $d_s = 1$ gives rise to the TM mode fields

$$\mathbf{E}_s^{\mathrm{TM}}(\mathbf{r}) = \mathbf{N}_s(\mathbf{r}), \tag{14}$$

$$\mathbf{H}_s^{\mathrm{TM}}(\mathbf{r}) = -\frac{\mathrm{i}k}{\omega\mu}\mathbf{M}_s(\mathbf{r}). \tag{15}$$

Two examples of transverse electric and magnetic vector modes are illustrated in figures 1 and 2. In figure 1 we show:

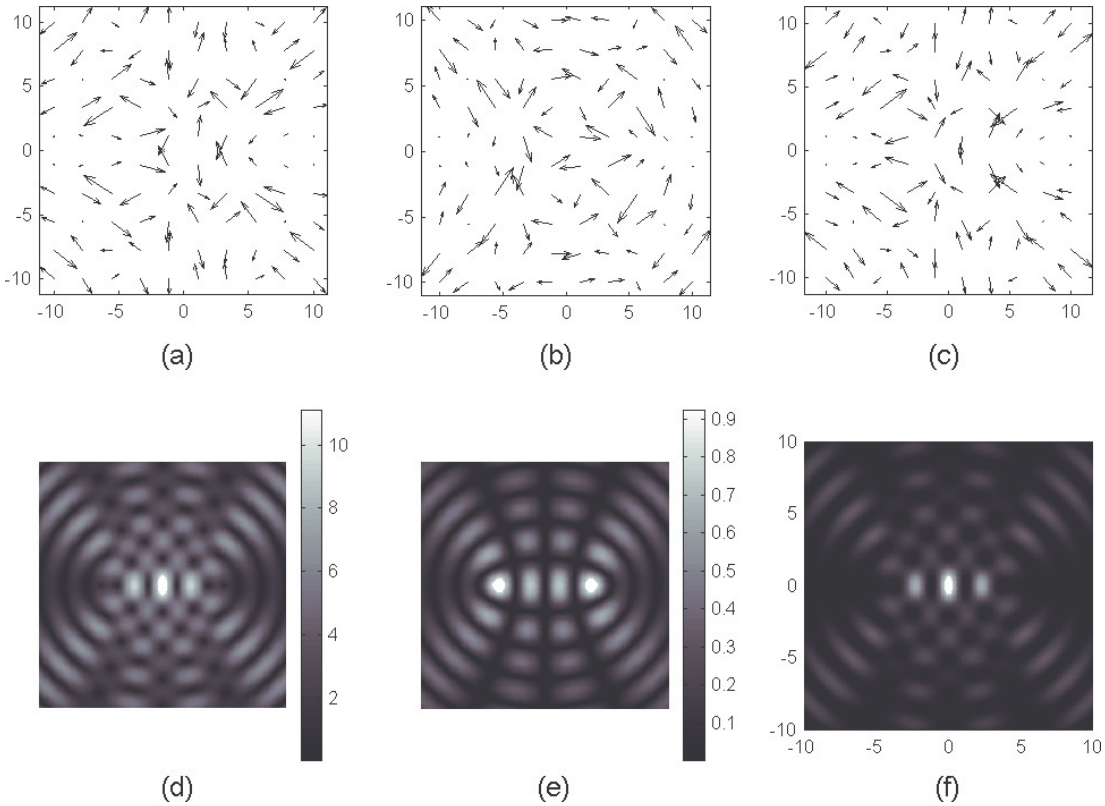

Figure 3. 'Left-handed' circularly polarized Mathieu beam derived from (18) associated with the even-type scalar field $\phi_3^{(e)}(u, v) = Je_3(u)ce_3(v)$, with parameters $k_t/k_z = 0.25$ and $f = 5\lambda$. (a)–(c) Vector diagrams of the transverse component of the electric field at three different instants: $t = 0$, $t = 0.25$ and $t = 0.5$, respectively, in units of $2\pi/\omega$. (d) and (e) Magnitude of the transverse and axial components of the electric field, respectively. Side bars illustrate the relative magnitudes. (f) Total intensity distribution. Length scales in units of λ.

(a) the instant vector diagram ($t = 0$) of the electric field for a TE mode (or magnetic field of TM mode) associated with the even-type Mathieu scalar PIOF $\phi_3^{(e)}(u, v) = Je_3(u)ce_3(v)$ and focal semi-axis $f = 5\lambda$; and (b) the transverse intensity distribution. In figure 2 we show: (a) the instant vector diagram and (b) magnitude of the transverse component of electric field ($\mathrm{Re}\{\mathbf{E}_\perp\} = \mathrm{Re}\{E_{q_1}\hat{\mathbf{e}}_1 + E_{q_2}\hat{\mathbf{e}}_2\}$ and $|\mathbf{E}_\perp| = (|E_{q_1}|^2 + |E_{q_2}|^2)^{1/2}$, respectively) for a TM mode (or magnetic field for TE mode) associated with the odd-type Mathieu scalar PIOF $\phi_2^{(o)}(u, v) = Jo_2(u)se_2(v)$ and $f = 6.25\lambda$; (c) the magnitude of the axial component of the field ($|\mathbf{E}_z|$) and (d) the total intensity distribution ($I = |\mathbf{E}_\perp|^2 + |\mathbf{E}_z|^2$) at a fixed z plane. In both examples $k_t/k_z = 0.25$. Also, notice that the field orientation remains constant at each point and its magnitude oscillates in time. Here Je_s and ce_s (Jo_s and se_s) represent the radial and angular even (odd) Mathieu functions, respectively, and the label s is a natural number *counting* the eigenvalue associated to a particular set of functions. It is convenient to stress at this point that the eigenvalues for even (a_s) and odd (b_s) Mathieu functions are different ($a_s \neq b_s$), even for the same value of s.

It is interesting to rewrite (10) and (11) in the circular polarization basis ($\hat{\mathbf{e}}_+, \hat{\mathbf{e}}_-, \hat{\mathbf{e}}_z$), using equations (A.9) and (A.11) from appendix A, and expressing the results in terms of the differential operators $\hat{U}^\pm$, defined in (A.12):

$$\mathbf{M}_s(\mathbf{r}) = \mathrm{i}k_t\left[\hat{\mathbf{e}}_+\hat{U}^- - \hat{\mathbf{e}}_-\hat{U}^+\right]\phi_s(\boldsymbol{\rho})\exp\{\mathrm{i}k_z z\}\,; \tag{16}$$

$$\mathbf{N}_s(\mathbf{r}) = \mathrm{i}k_z\frac{k_t}{k}\left[\hat{\mathbf{e}}_+\hat{U}^- + \hat{\mathbf{e}}_-\hat{U}^+ - \mathrm{i}\frac{k_t}{k_z}\hat{\mathbf{e}}_z\right]\phi_s(\boldsymbol{\rho})\exp\{\mathrm{i}k_z z\}\,. \tag{17}$$

This suggests the combinations to eliminate the $\hat{\mathbf{e}}_+$ or the $\hat{\mathbf{e}}_-$ components, which at the level of (7), (12) and (14) correspond to

$$\mathbf{E}_s^{\mathrm{L}}(\mathbf{r}) = \mathbf{E}_s^{\mathrm{TE}} + \frac{k}{k_z}\mathbf{E}_s^{\mathrm{TM}} = \mathrm{i}k_t\left[2\hat{\mathbf{e}}_+\hat{U}^- - \mathrm{i}\frac{k_t}{k_z}\hat{\mathbf{e}}_z\right] \times \phi_s(\boldsymbol{\rho})\exp\{\mathrm{i}k_z z\}\,; \tag{18}$$

$$\mathbf{E}_s^{\mathrm{R}}(\mathbf{r}) = -\mathbf{E}_s^{\mathrm{TE}} + \frac{k}{k_z}\mathbf{E}_s^{\mathrm{TM}} = \mathrm{i}k_t\left[2\hat{\mathbf{e}}_-\hat{U}^+ - \mathrm{i}\frac{k_t}{k_z}\hat{\mathbf{e}}_z\right] \times \phi_s(\boldsymbol{\rho})\exp\{\mathrm{i}k_z z\}\,. \tag{19}$$

The transverse components can be identified as left and right 'circular polarization' states; but of course, both fields also have the common longitudinal component. The associated magnetic fields at the level of equations (8), (13) and (15) follow from the respective linear combinations, which are not written here explicitly for the sake of space. It is recognized that the electric and magnetic fields of each 'circularly polarized' state are not orthogonal $\mathbf{E}_s^i \cdot \mathbf{H}_s^i \neq 0$ for $i = \mathrm{L}, \mathrm{R}$.

Figure 3 illustrates the case of a 'left-handed' circularly polarized Mathieu beam associated with the even-type scalar function $\phi_3^{(e)}(u, v) = Je_3(u)ce_3(v)$ with $f = 5\lambda$. Frames (a)–(c) show vector diagrams of the transverse component of the electric field at three different instants: $t = 0$, $t = 0.25$ and

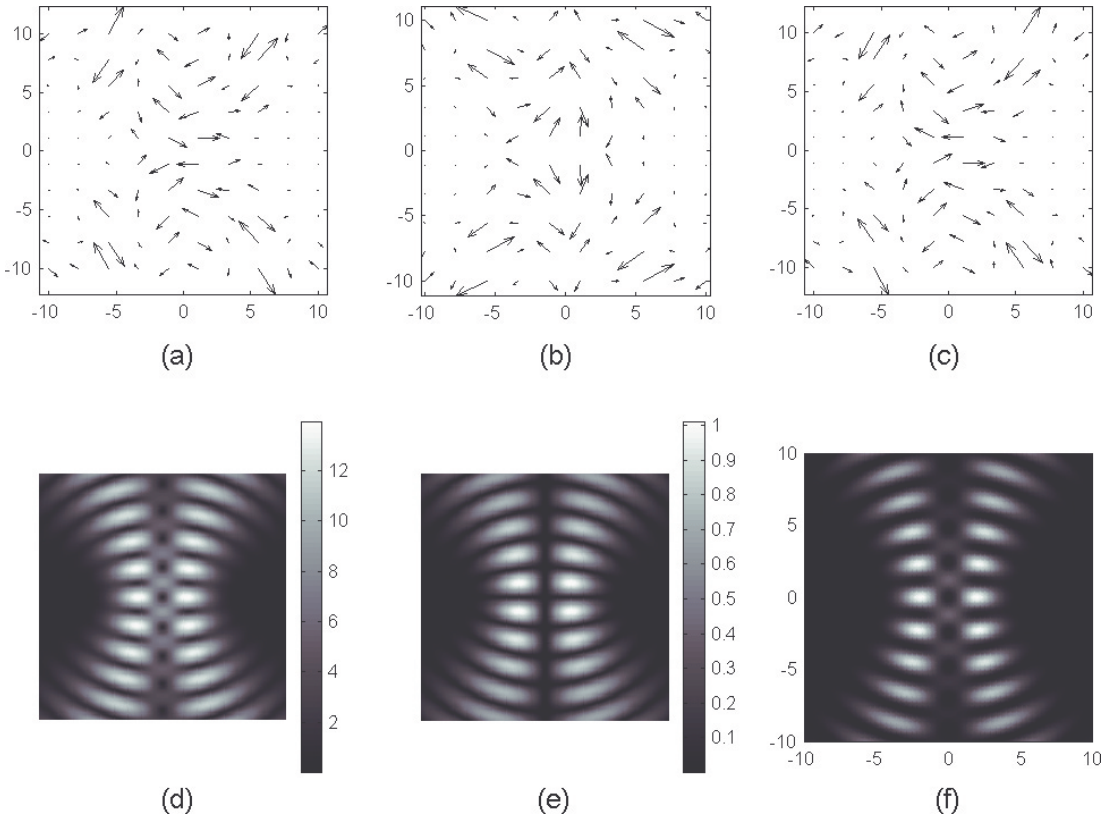

Figure 4. 'Right-handed' circularly polarized Mathieu beam derived from (19) associated with the odd-type scalar field $\phi_2^{(o)}(u, v) = Jo_2(u)se_2(v)$ with $k_t/k_z = 0.25$ and $f = 6.25\lambda$. (a)–(c) Vector diagrams of the transverse component of the electric field at three different instants: $t = 0$, $t = 0.25$ and $t = 0.5$, respectively, in units of $2\pi/\omega$. (d) and (e) Magnitude of the transverse and axial components of the electric field, respectively. (f) Total intensity distribution. Length scales in units of λ.

$t = 0.5$, respectively, in units of $2\pi/\omega$. Frames (d) and (e) show the magnitude of the transverse and axial components of the electric field, respectively, and (f) corresponds to the total intensity distribution. On the other hand, figure 4 shows the same quantities for a 'right-handed' polarized Mathieu beam associated with the odd-type scalar function $\phi_2^{(o)}(u, v) = Jo_2(u)se_2(v)$ with $f = 6.25\lambda$. In both examples $k_t/k_z = 0.25$. Following the established convention [19], at a given z plane, it can be seen that the transverse components of the fields rotate anti-clockwise (clockwise) for left- (right-) handed circular polarization as t varies.

2.2. *'Circularly polarized' states*

For the selections of the unit vector $\hat{\mathbf{a}} = \pm\hat{\mathbf{e}}_\pm$ and the scalar PIOF $\Psi_s(\mathbf{r}) = \psi_s(\boldsymbol{\rho})\exp(\mathrm{i}k_z z)$, (4) and (5) become

$$\mathbf{M}_s^\pm = k_z\left[\hat{\mathbf{e}}_\pm + \mathrm{i}\frac{k_t}{k_z}\hat{\mathbf{e}}_z\hat{U}^\pm\right]\psi_s(\rho)\exp\{\mathrm{i}k_z z\}, \tag{20}$$

$$\mathbf{N}_s^\pm = \pm\left[k\hat{\mathbf{e}}_\pm + \frac{k_t}{k}\hat{U}^\pm\nabla\right]\psi_s(\boldsymbol{\rho})\exp\{\mathrm{i}k_z z\}, \tag{21}$$

using (A.11) and (A.13) successively. Notice that while the $\mathbf{M}_s^\pm$ fields have only two components in the $(\hat{\mathbf{e}}_+, \hat{\mathbf{e}}_-, \hat{\mathbf{e}}_z)$ basis, the $\mathbf{N}_s^\pm$ fields have three components.

In this case, we identify left and right 'circularly polarized' states as

$$\mathbf{E}_s^\pm = \mathbf{M}_s^\pm, \tag{22}$$

$$\mathbf{H}_s^\pm = -\frac{\mathrm{i}k}{\mu\omega}\mathbf{N}_s^\pm, \tag{23}$$

in which the electric and magnetic fields are not orthogonal. The quotation marks are used in the adjective circularly polarized recognizing that the corresponding vector PIOFs also have longitudinal components.

Left- and right-handed 'circular polarization' states defined by (20) and (22), corresponding to the plus and minus signs in the superindices, are exemplified in figures 5 and 6 for Mathieu beams associated to the scalar fields $\psi_3^{(e)}(u, v) = Je_3(u)ce_3(v)$ and $\psi_2^{(o)}(u, v) = Jo_2(u)se_2(v)$, respectively, at three different instants: $t = 0.125$, $t = 0.25$ and $t = 0.375$, all the other parameters being the same as those of figures 3 and 4. Notice that the transverse component of the electric field vector in figures 5 and 6 has the same orientation at each point of the space for a given time, in contrast with the circularly polarized states derived from the TE and TM modes (figures 3 and 4). The rotation in time of the transverse electric field vector according to the established convention of circular polarizations in each case becomes apparent.

Other polarization states can be constructed by superposing those defined by (22), namely,

$$\begin{aligned}\mathbf{E}_s^\pm &= A_1\mathbf{M}_s^+ + A_2\mathbf{M}_s^- \\ &= k_z\left[\left(A_1\hat{\mathbf{e}}_+ + A_2\hat{\mathbf{e}}_-\right) + \mathrm{i}\frac{k_t}{k_z}\hat{\mathbf{e}}_z\left(A_1\hat{U}^+ + A_2\hat{U}^-\right)\right] \\ &\quad\times\psi_s(\boldsymbol{\rho})\exp\{\mathrm{i}k_z z\}.\end{aligned} \tag{24}$$

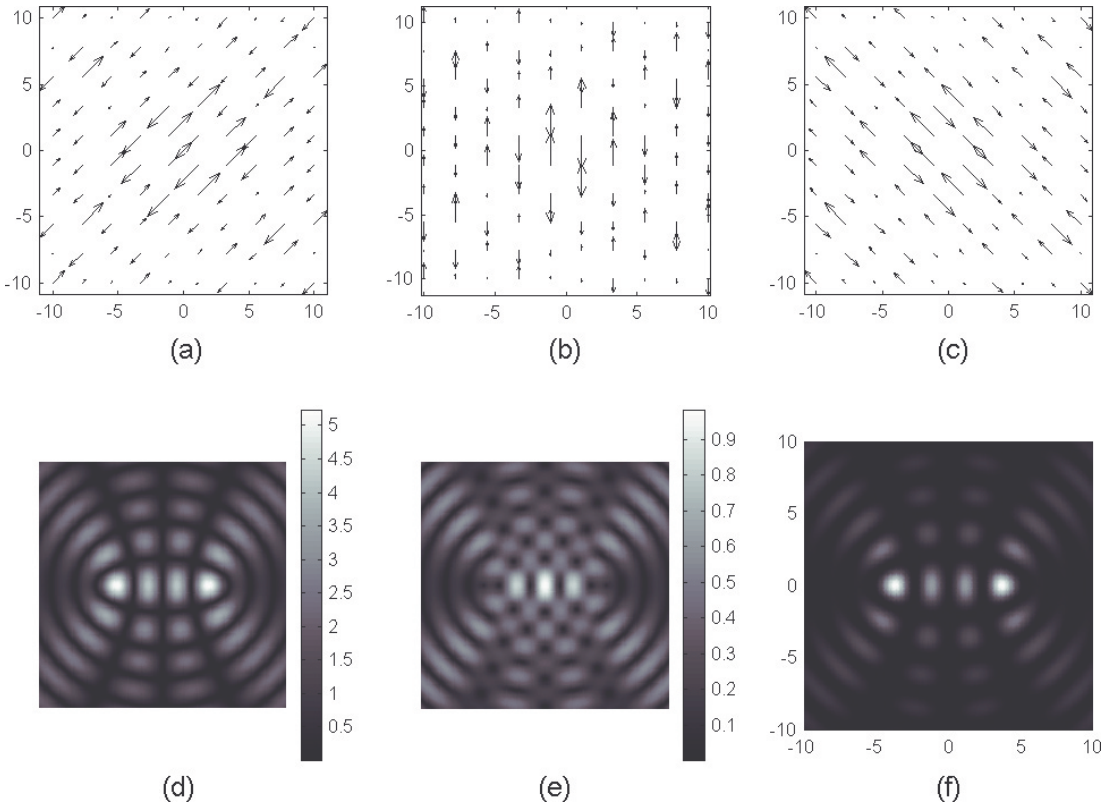

Figure 5. 'Left-handed' circularly polarized Mathieu beam derived from (20) and (22) (plus sign of superindex) associated with the even-type scalar field $\psi_3^{(e)}(u, v) = Je_3(u)ce_3(v)$ with $k_t/k_z = 0.25$ and $f = 5\lambda$: (a)–(c) Vector diagrams of the transverse component of the electric field at three different instants: $t = 0.125$, $t = 0.25$ and $t = 0.375$, respectively, in units of $2\pi/\omega$. (d) and (e) Magnitude of the transverse and axial components of the electric field, respectively. (f) Total intensity distribution. Length scales in units of λ.

It is straightforward to demonstrate that a 'linearly polarized' state follows by choosing

$$A_1 = \frac{1}{\sqrt{2}}(B_1 - \mathrm{i}B_2)\,; \qquad A_2 = A_1^*, \tag{25}$$

where B_1 and B_2 are real constants such that $B_1^2 + B_2^2 = 1 = |A_1|^2 + |A_2|^2$. The polarization plane is defined by the angle $\theta = \tan^{-1}(B_2/B_1)$ measured from the positive x-axis.

Notice that, in the paraxial limit (corresponding in this case to $k_t \ll k_z \approx k$), the longitudinal components of the left- and right-handed circularly polarized states, as well as for the linear polarization state, become negligible.

3. Connections between polarization bases

In section 2.1 the left and right 'circular polarization' states of (18) and (19) were constructed as superpositions of TE and TM modes. In section 2.2 the alternative left and right 'circularly polarized' states of (20)–(23) were directly constructed and identified; their superpositions, (24), leading to 'linear polarization' states with the choice of coefficients of (25) were also identified.

Comparison of the respective 'circular polarization' states of (18) and (19), and (20)–(23) allows us to identify the connections between them. In fact, such connections between the respective scalar PIOFs are

$$\phi_s = \hat{U}^{\pm}\psi_s, \tag{26}$$

in order to go from the first set to the second one, and

$$\psi_s = -\hat{U}^{\mp}\phi_s, \tag{27}$$

for going from the second to the first. Here we used the fact that $\nabla_\perp^2 = 2k_t^2\hat{U}^+\hat{U}^-$ (equation (A.13), appendix A).

The connections given by (26) and (27) become apparent in figures 3 and 5, since the transverse component of the field in figure 3 corresponds to the axial component in figure 5 and vice versa, and the same occurs between figures 4 and 6.

The two sets of polarization bases are of great importance in optics. On the one hand, the TE and TM modes discussed in section 2.1 are the typical propagation modes arising in bounded media like optical fibres [13, 20], although they can also be generated in free space with interferometric techniques [15]. On the other hand, the sets discussed in section 2.2 are the kind of fields usually generated in the laboratory for free space or linear isotropic media (see for example [11, 14]), and correspond *in the paraxial limit* to the so-called scalar solutions.

4. Dynamical properties

The electromagnetic field vectors constructed for two different polarization basis in section 2 lead directly to the corresponding expressions for the energy density and Poynting vector. This will allow us not only to analyse the propagation

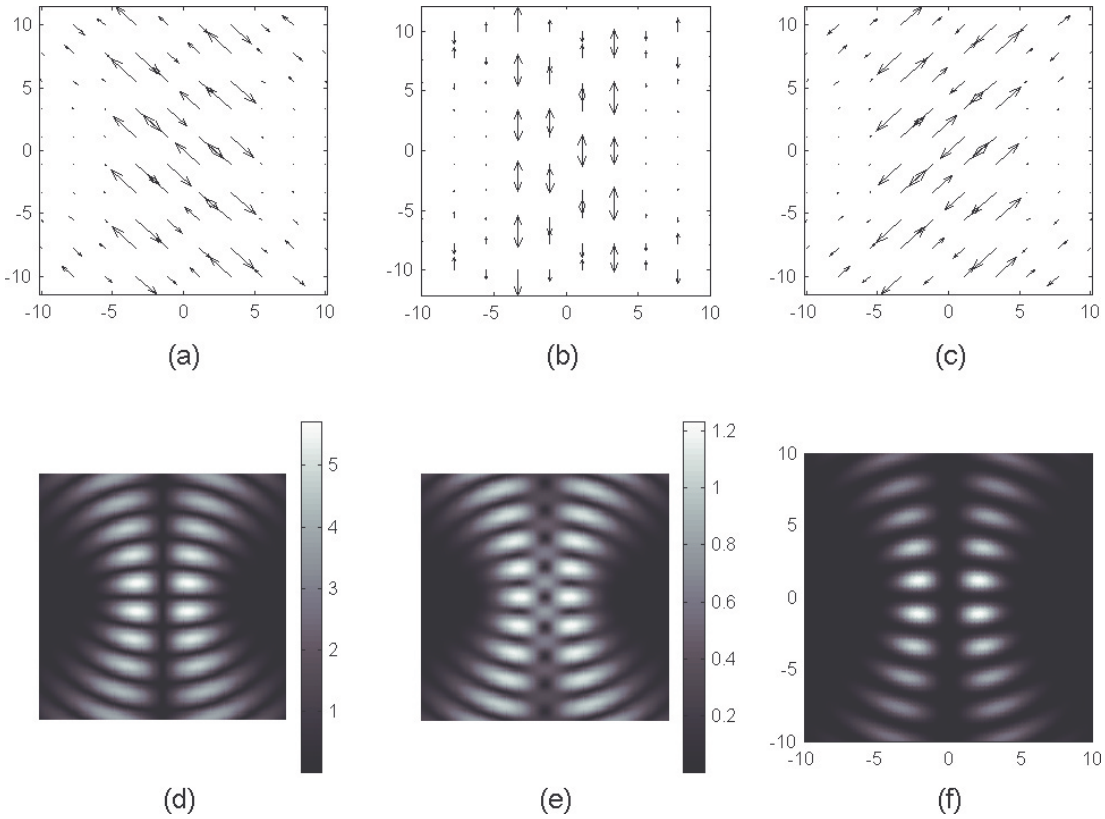

Figure 6. 'Right-handed' circularly polarized Mathieu beam derived from (20) and (22) (minus sign of superindex) associated with the odd-type scalar field $\psi_2^{(o)}(u, v) = Jo_2(u)se_2(v)$ with $k_t/k_z = 0.25$ and $f = 6.25\lambda$. (a)–(c) Vector diagrams of the transverse component of the electric field at three different instants: $t = 0.125$, $t = 0.25$ and $t = 0.375$, respectively, in units of $2\pi/\omega$. (d) and (e) Magnitude of the transverse and axial components of the electric field, respectively. (f) Total intensity distribution. Length scales in units of λ.

invariant condition for vector fields, but also to study some basic dynamical properties of PIOFs.

The energy density for the transverse modes, TE or TM, is given by

$$w = \frac{\epsilon}{4}\left[\left(1+\frac{k_z^2}{k^2}\right)|\nabla_\perp\phi_s|^2 + \frac{k_t^4}{k^2}|\phi_s|^2\right]. \tag{28}$$

And the time averaged Poynting vector in this case is given by

$$\langle \mathbf{S}\rangle = \frac{c\epsilon}{2}\left[\frac{k_z}{k}|\nabla_\perp\phi_s|^2\,\hat{\mathbf{e}}_z - \frac{k_t^2}{k^2}\,\mathrm{Re}\left\{\mathrm{i}\phi_s\nabla_\perp\phi_s^*\right\}\right]. \tag{29}$$

From (29) it can immediately be seen that when ϕ_s is real, the Poynting vector has axial component only, whereas for ϕ_s complex the energy flux will have a transverse component. In the case of Bessel beams, for example, this establishes the difference between standing ($J_m(k_t\rho)\cos m\varphi$, $J_m(k_t\rho)\sin m\varphi$) and rotating ($J_m(k_t\rho)\exp\{\pm \mathrm{i}m\varphi\}$) transverse modes; the transverse component of the energy flux for the case of rotating modes is purely tangential and it is associated to the orbital angular momentum carried by these beams [11]. In the case of elliptic and parabolic symmetries, the respective conserved dynamical quantities that play an analogous role to the orbital angular momentum are identified in [18].

On the other hand, the calculation of the energy density for the 'circularly polarized' fields of section 2.2, defined by (20)–(23), leads to

$$w^{\pm} = \frac{\epsilon}{4}\frac{k_z^4}{k^2}\left[\left(2+2\frac{k_t^2}{k_z^2}+\frac{k_t^4}{4k_z^4}\right)|\psi_s|^2 + \frac{k_t^2}{k_z^2}\left(2+\frac{k_t^2}{k_z^2}\right) \times (\hat{U}^{\pm}\psi_s)(\hat{U}^{\mp}\psi_s^*) + \frac{k_t^4}{k_z^4}\{(\hat{U}^{\pm})^2\psi_s\}\{(\hat{U}^{\mp})^2\psi_s^*\}\right] \tag{30}$$

and the Poynting vector

$$\langle \mathbf{S}^{\pm}\rangle = \frac{c\epsilon}{2}\frac{k_z^3}{k}\left(\hat{\mathbf{e}}_z\left[1+\frac{k_t^2}{2k_z^2}\right]|\psi_s|^2 + 2\frac{k_t}{k_z}\left[1+\frac{k_t^2}{4k_z^2}\right]\mathrm{Im}\{\hat{\mathbf{e}}_{\mp}\psi_s^*\hat{U}^{\pm}\psi_s\} - \frac{k_t^3}{k_z^3}\,\mathrm{Im}\{\hat{\mathbf{e}}_{\pm}(\hat{U}^{\pm}\psi_s)[(\hat{U}^{\mp})^2\psi_s^*]\}\right). \tag{31}$$

The expressions for the energy density and Poynting vector for the 'circularly polarized' basis defined in (18) and (19) can be obtained respectively from expressions (30) and (31) by applying the transformation (27). In contrast with the TE and TM modes, for 'circularly polarized' modes the energy flux will always possess both longitudinal and transverse components, regardless of the nature of the scalar function ψ_s (real or complex).

The propagation invariance nature of vector Bessel PIOFs has been established based on different conditions in [10] and [21], which are not in contradiction to each other. The conditions proposed in [10] are more specific, while those

in [21] are simpler. For our present discussion, the latter are more direct, and can be generalized for any family of PIOFs as

$$\begin{aligned} w(q_1, q_2, z > 0) &= w(q_1, q_2, z = 0), \\ S_z(q_1, q_2, z > 0) &= S_z(q_1, q_2, z = 0), \end{aligned} \tag{32}$$

where S_z denotes the z-component of the Poynting vector. It can be seen from (28), (29) and (30), (31) that all the vector fields analysed in this work are propagation invariant according to the definition (32).

5. Discussion

Vector propagation invariant optical fields have been constructed in section 2 of this paper, by using Stratton's general method [17] with appropriately chosen unit vectors and scalar PIOF solutions of the Helmholtz equation. Specifically in section 2.1, the choice of the unit vector in the longitudinal direction leads to the transverse electromagnetic TE and TM modes of equations (12), (13) and (14), (15), respectively. Left- and right-handed 'circular polarization' states were also constructed as the superpositions of TE and TM modes of equations (18) and (19). On the other hand, the alternative choice of the 'circular polarization' unit vectors $\hat{\mathbf{e}}_\pm$ in section 2.2 led to the corresponding PIOF states of equations (20) and (23). Their superpositions in equation (24) describe other possible polarization states. The connections between the respective 'circular polarization' states are exhibited via equations (26) and (27) in section 3, as the connections between the respective scalar PIOFs. Section 4 contains the expressions of energy density and Poynting vector for the TE and TM modes, (28) and (29), and for the 'circular polarization' states of section 2.2, (30), (31), showing their PIOF nature. It is important to point out that the treatment shown here is completely general in the sense that it does not depend on the specific coordinate system (rectangular, circular, elliptic or parabolic cylindrical coordinates), so it can be applied to any family of PIOFs.

In the paraxial limit ($k_t \ll k_z \approx k$), the equations presented in section 2.2 reduce to the equations that can be obtained from the scalar approach. The longitudinal components of the electric and magnetic fields can be neglected and the corresponding vectors indeed become orthogonal for any polarization basis.

The previous experience with the case of Bessel beams shows that important information about the different polarization and dynamical properties of these light fields can only be obtained from the rigorous vectorial approach. Specifically, it has been recently demonstrated that vector vortices with TE and TM polarizations can be generated in free space [15] based on the full vector description of PIOFs described in section 2.1, which exhibit different properties compared with the scalar vortices [11, 22] obtained from the polarization basis studied in section 2.2 in the paraxial limit.

On the other hand, in analogy with the case of rotating Bessel beams, $J_m(k_t\rho)\exp\{\pm \mathrm{i}m\varphi\}$, complex linear superpositions of Mathieu beams labelled as travelling or helical modes have been constructed in the scalar version [23, 24] with the form

$$\begin{aligned} U(u, v, z) &= C_s(f)Je_s(u; f, a_s)ce_s(v; f) \\ &\pm \mathrm{i}S_s(f)Jo_s(u; f, b_s)se_s(v; f, b_s), \end{aligned} \tag{33}$$

where $C_s(f)$ and $S_s(f)$ represent weighting constants that depend on the interfocal distance f (related to the parameter $q = f^2k_t^2/4$ in [23, 24]). Here we include the explicit dependence of the even and odd functions on their respective eigenvalues, a_s and b_s, in order to point out that the components of such superpositions are associated with different eigenvalues $a_s \neq b_s$. Only in the case of Bessel beams do the even and odd angular standing solutions of the scalar Helmholtz equation ($J_m(k_t\rho)\cos m\varphi$ and $J_m(k_t\rho)\sin m\varphi$, respectively) share the same eigenvalue, m. Therefore, the optical field described by (33) does not possess a *well defined angular momentum state*, which means that, although the optical angular momentum density can indeed be calculated for this [25] or any other kind of electromagnetic field according to definitions provided by fundamental electrodynamics [26], a quantity such as an optical angular momentum per photon cannot be associated to those fields. In contrast with any optical wavefield having a dependence of the form $\exp\{\pm \mathrm{i}m\varphi\}$, Mathieu beams are not eigenstates of the operator associated with the z-component of the orbital angular momentum, $\frac{\partial}{\partial\varphi}$. Their behaviour in interaction with microscopic particles, however, shows interesting features by itself [24].

Similar comments could be made about the so-called 'travelling solutions' of parabolic non-diffracting beams [5]. In that sense, the formalism developed here allows us to appreciate that complex linear superpositions of PIOFs sharing the same eigenvalue, and hence having a well defined dynamical state, can be constructed as $\hat{U}^{\pm}\psi_s$, in any of the cylindrical geometries.

In conclusion, this paper provides several complete vector bases of PIOFs, each one with well defined polarization properties, including the circular, elliptic and parabolic varieties determined by the associated geometries. These bases are of optical interest by themselves, and are on a par with the familiar plane wave bases. The experience with the Bessel beams—in their scalar and vector versions, and their numerous applications—can be extended to Mathieu and Weber beams. The results presented herein are fundamental steps in the general scalar to vector extension. They are proper tools for future steps like vector versions of [6–8] and the polarization and invariants of real electromagnetic beams *a la* [12, 27, 28], expressed as superpositions of vector PIOFs.

Acknowledgments

The authors wish to thank the referees for useful comments to improve this manuscript. This work was partially supported by DGAPA-UNAM project IN103103.

Appendix A. Circular polarization basis

The circularly polarized and Cartesian vector bases are related by

$$\hat{\mathbf{e}}_\pm = \frac{\hat{\mathbf{e}}_x \pm \mathrm{i}\hat{\mathbf{e}}_y}{\sqrt{2}}, \qquad \hat{\mathbf{e}}_z = \hat{\mathbf{e}}_z \tag{A.1}$$

and vice versa

$$\hat{\mathbf{e}}_x = \frac{\hat{\mathbf{e}}_+ + \hat{\mathbf{e}}_-}{\sqrt{2}}; \qquad \hat{\mathbf{e}}_y = \frac{\hat{\mathbf{e}}_+ - \hat{\mathbf{e}}_-}{\sqrt{2}\mathrm{i}}. \tag{A.2}$$

The scalar products of the unit vectors in (A.1) are

$$\hat{\mathbf{e}}_\pm \cdot \hat{\mathbf{e}}_\pm = \hat{\mathbf{e}}_\pm \cdot \left(\hat{\mathbf{e}}_\mp\right)^* = 0; \qquad \hat{\mathbf{e}}_\pm \cdot \hat{\mathbf{e}}_\mp = \hat{\mathbf{e}}_\pm \cdot \left(\hat{\mathbf{e}}_\pm\right)^* = 1; \qquad \hat{\mathbf{e}}_\pm \cdot \hat{\mathbf{e}}_z = 0; \qquad \hat{\mathbf{e}}_z \cdot \hat{\mathbf{e}}_z = 1. \tag{A.3}$$

Their cross products are given as

$$\hat{\mathbf{e}}_\pm \times \hat{\mathbf{e}}_\mp = \mp\hat{\mathbf{e}}_z; \qquad \hat{\mathbf{e}}_\pm \times \hat{\mathbf{e}}_\pm = 0; \qquad \hat{\mathbf{e}}_\pm \times \hat{\mathbf{e}}_z = \pm \mathrm{i}\hat{\mathbf{e}}_\pm. \tag{A.4}$$

Any vector can be expressed in the basis of (A.1) as

$$\mathbf{V} = \hat{\mathbf{e}}_+ V_- + \hat{\mathbf{e}}_- V_+ + \hat{\mathbf{e}}_z V_z, \tag{A.5}$$

where

$$V_\pm = \frac{V_x \pm \mathrm{i} V_y}{\sqrt{2}}. \tag{A.6}$$

Then the scalar and vector products of two vectors take the respective forms

$$\mathbf{V} \cdot \mathbf{W} = V_- W_+ + V_+ W_- + V_z W_z, \tag{A.7}$$

and

$$\mathbf{V} \times \mathbf{W} = \mathrm{i}\hat{\mathbf{e}}_+ (V_- W_z - V_z W_-) + \mathrm{i}\hat{\mathbf{e}}_- (V_z W_+ - V_+ W_z) + \mathrm{i}\hat{\mathbf{e}}_z (V_+ W_- - V_- W_+). \tag{A.8}$$

The gradient of a scalar function is given by

$$\nabla f = \hat{\mathbf{e}}_+ \frac{1}{\sqrt{2}} \left(\frac{\partial}{\partial x} - \mathrm{i}\frac{\partial}{\partial y} \right) f + \hat{\mathbf{e}}_- \frac{1}{\sqrt{2}} \left(\frac{\partial}{\partial x} + \mathrm{i}\frac{\partial}{\partial y} \right) f + \hat{\mathbf{e}}_z \frac{\partial f}{\partial z}. \tag{A.9}$$

The divergence of a vector field becomes

$$\nabla \cdot \mathbf{V} = \frac{1}{\sqrt{2}} \left(\frac{\partial}{\partial x} - \mathrm{i}\frac{\partial}{\partial y} \right) V_+ + \frac{1}{\sqrt{2}} \left(\frac{\partial}{\partial x} + \mathrm{i}\frac{\partial}{\partial y} \right) V_- + \frac{\partial V_z}{\partial z}. \tag{A.10}$$

And the curl of the vector field is expressed as

$$\nabla \times \mathbf{V} = \mathrm{i}\hat{\mathbf{e}}_+ \left[\frac{1}{\sqrt{2}} \left(\frac{\partial}{\partial x} - \mathrm{i}\frac{\partial}{\partial y} \right) V_z - \frac{\partial V_-}{\partial z} \right] + \mathrm{i}\hat{\mathbf{e}}_- \left[\frac{\partial V_+}{\partial z} - \frac{1}{\sqrt{2}} \left(\frac{\partial}{\partial x} + \mathrm{i}\frac{\partial}{\partial y} \right) V_z \right] + \mathrm{i}\hat{\mathbf{e}}_z \frac{1}{\sqrt{2}} \left[\left(\frac{\partial}{\partial x} + \mathrm{i}\frac{\partial}{\partial y} \right) V_- - \left(\frac{\partial}{\partial x} - \mathrm{i}\frac{\partial}{\partial y} \right) V_+ \right]. \tag{A.11}$$

Notice the presence of the same combinations

$$\frac{1}{\sqrt{2}} \left(\frac{\partial}{\partial x} \pm \mathrm{i}\frac{\partial}{\partial y} \right) \equiv k_t \hat{U}^\pm \tag{A.12}$$

in the derivatives of (A.9)–(A.11), justifying the introduction of the $\hat{U}^\pm$ operators used in section 2.

The Laplace operator takes the forms

$$\nabla^2 = k_t^2 \left(\hat{U}^+ \hat{U}^- + \hat{U}^- \hat{U}^+ \right) + \frac{\partial^2}{\partial z^2} = 2k_t^2 \hat{U}^+ \hat{U}^- + \frac{\partial^2}{\partial z^2} = 2k_t^2 \hat{U}^- \hat{U}^+ + \frac{\partial^2}{\partial z^2}, \tag{A.13}$$

taking into account the commutativity of the $\hat{U}^+$ and $\hat{U}^-$ operators.

Appendix B. Cylindrical coordinate systems

Circular (ρ, φ, z), elliptical (u, v, z) and parabolic (ξ, η, z) cylindrical coordinates are defined via their connections with the Cartesian coordinates [29], respectively:

$$x = \rho \cos\varphi; \qquad y = \rho \sin\varphi; \qquad z = z, \tag{B.1}$$

$$x = f \cosh u \cos v; \qquad y = f \sinh u \sin v; \qquad z = z, \tag{B.2}$$

$$x = \frac{\xi^2 - \eta^2}{2}; \qquad y = \xi\eta; \qquad z = z, \tag{B.3}$$

where $\rho \in [0, \infty)$, $\varphi \in [0, 2\pi)$, $u \in [0, \infty)$, $v \in [0, 2\pi)$, $\xi \in [-\infty, \infty)$ and $\eta \in [0, \infty)$.

Any differential displacement in the three-dimensional space can be evaluated in the successive coordinates, taking the respective forms

$$\begin{aligned} d\vec{\mathbf{r}} &= \hat{\mathbf{e}}_x \, dx + \hat{\mathbf{e}}_y \, dy + \hat{\mathbf{e}}_z \, dz \\ &= h_\rho \, d\rho \hat{\mathbf{e}}_u + h_\varphi \, d\varphi \hat{\mathbf{e}}_v + \hat{\mathbf{e}}_z \, dz \\ &= h_u \, du \hat{\mathbf{e}}_u + h_v \, dv \hat{\mathbf{e}}_v + \hat{\mathbf{e}}_z \, dz \\ &= h_\xi \, d\xi \hat{\mathbf{e}}_\xi + h_\eta \, d\eta \hat{\mathbf{e}}_\eta + \hat{\mathbf{e}}_z \, dz, \end{aligned} \tag{B.4}$$

where the corresponding scale factors and unit vectors are identified to be

$$h_\rho = 1, \qquad h_\varphi = \rho, \tag{B.5}$$

$$h_u = h_v = f\sqrt{\cosh^2 u - \cos^2 v}, \tag{B.6}$$

$$h_\xi = h_\eta = \sqrt{\xi^2 + \eta^2}, \tag{B.7}$$

and

$$\hat{\mathbf{e}}_\rho = \hat{\mathbf{e}}_x \cos\varphi + \hat{\mathbf{e}}_y \sin\varphi, \qquad \hat{\mathbf{e}}_\varphi = -\hat{\mathbf{e}}_x \sin\varphi + \hat{\mathbf{e}}_y \cos\varphi, \tag{B.8}$$

$$\hat{\mathbf{e}}_u = \frac{f}{h_u} \left(\hat{\mathbf{e}}_x \sinh u \cos v + \hat{\mathbf{e}}_y \cosh u \sin v \right), \tag{B.9}$$

$$\hat{\mathbf{e}}_v = \frac{f}{h_u} \left(-\hat{\mathbf{e}}_x \cosh u \sin v + \hat{\mathbf{e}}_y \sinh u \cos v \right),$$

$$\hat{\mathbf{e}}_\xi = \frac{1}{h_\xi} \left(\hat{\mathbf{e}}_x \xi + \hat{\mathbf{e}}_y \eta \right), \qquad \hat{\mathbf{e}}_\eta = \frac{1}{h_\xi} \left(-\hat{\mathbf{e}}_x \eta + \hat{\mathbf{e}}_y \xi \right). \tag{B.10}$$

Notice the orthogonality of the pair of vectors in the respective equations (B.8)–(B.10). The inverse transformations for the Cartesian unit vectors are

$$\hat{\mathbf{e}}_x = \hat{\mathbf{e}}_\rho \cos\varphi - \hat{\mathbf{e}}_\varphi \sin\varphi, \qquad \hat{\mathbf{e}}_y = \hat{\mathbf{e}}_\rho \sin\varphi + \hat{\mathbf{e}}_\varphi \cos\varphi, \tag{B.11}$$

$$\hat{\mathbf{e}}_x = \frac{f}{h_u} \left(\hat{\mathbf{e}}_u \sinh u \cos v - \hat{\mathbf{e}}_v \cosh u \sin v \right), \tag{B.12}$$

$$\hat{\mathbf{e}}_y = \frac{f}{h_u} \left(-\hat{\mathbf{e}}_u \cosh u \sin v + \hat{\mathbf{e}}_v \sinh u \cos v \right),$$

$$\hat{\mathbf{e}}_x = \frac{1}{h_\xi} \left(\hat{\mathbf{e}}_\xi \xi + \hat{\mathbf{e}}_\eta \eta \right), \qquad \hat{\mathbf{e}}_y = \frac{1}{h_\xi} \left(-\hat{\mathbf{e}}_\xi \eta + \hat{\mathbf{e}}_\eta \xi \right). \tag{B.13}$$

When the latter are substituted successively in (A.1), the circularly polarized basis vectors become, respectively,

$$\hat{\mathbf{e}}^\pm = \frac{\left(\hat{\mathbf{e}}_\rho \pm \mathrm{i}\hat{\mathbf{e}}_\varphi \right)}{\sqrt{2}} \exp\{\pm \mathrm{i}\varphi\}, \tag{B.14}$$

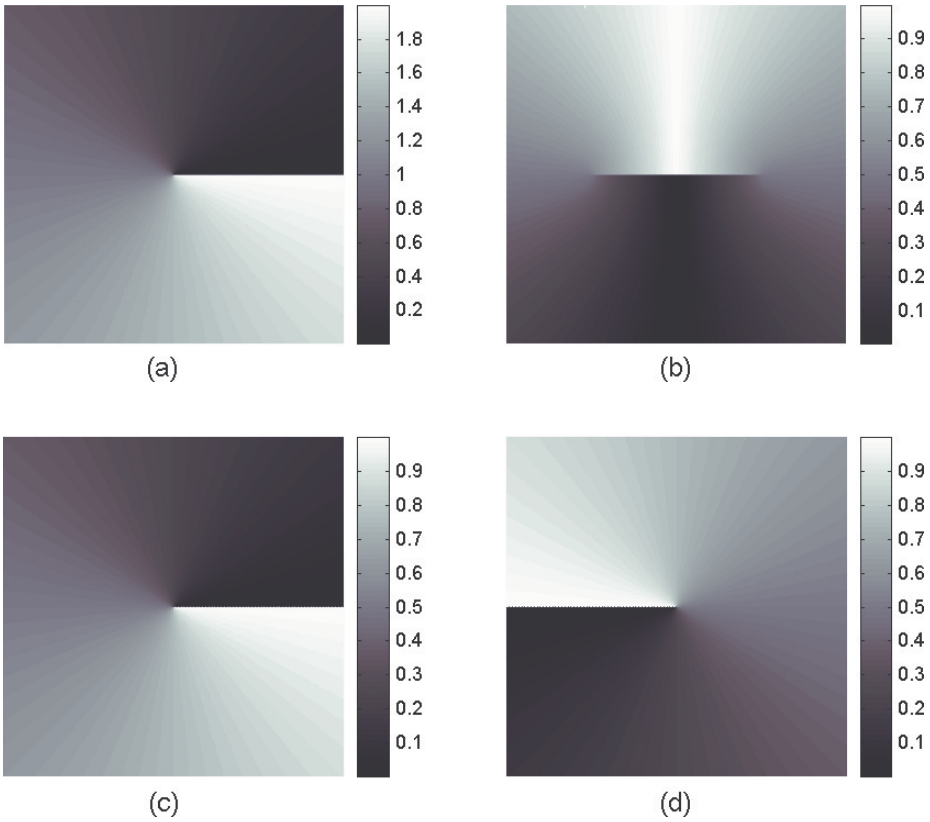

Figure B.1. Space distribution of the phases (a) φ, (b) α and (c) and (d) β, respectively, associated with the circular polarization vector basis for the three different coordinate systems, in units of π. The focal semi-axis for the case of elliptic coordinates (b) corresponds to 5 length units.

$$\hat{\mathbf{e}}^{\pm} = \frac{\left(\hat{\mathbf{e}}_u \pm \mathrm{i}\hat{\mathbf{e}}_v\right)}{\sqrt{2}} \exp\left\{\pm \mathrm{i}\alpha\,(u, v)\right\}, \tag{B.15}$$

$$\hat{\mathbf{e}}^{\pm} = \frac{\left(\hat{\mathbf{e}}_\xi \pm \mathrm{i}\hat{\mathbf{e}}_\eta\right)}{\sqrt{2}} \exp\left\{\pm \mathrm{i}\beta\,(\xi, \eta)\right\}, \tag{B.16}$$

where

$$\alpha(u, v) = \arcsin\left(\frac{f \cosh u \sin v}{h_u}\right),$$

$$\beta(\xi, \eta) = \arcsin\left(\frac{\eta}{h_\xi}\right) = \frac{\varphi}{2}.$$

Figure B.1 shows the space distribution of respective phases φ, α and β associated with the circular polarization basis for the three different coordinate systems. Notice that the respective branch cuts in the different segments of the x-axis: (a) $(0 < \rho < \infty, \varphi = 0)$ for circular, (b) the interfocal segment $(u = 0, 0 \leqslant v < 2\pi)$ for elliptic and (c) $(\xi^2 > \eta^2, \eta = 0)$ and (d) $(\xi^2 < \eta^2, \eta = 0)$ for parabolic coordinates.

The Cartesian transverse derivatives can also be translated in the respective curvilinear coordinates, taking the forms

$$\frac{\partial}{\partial x} = \cos\varphi \frac{\partial}{\partial \rho} - \frac{\sin\varphi}{\rho}\frac{\partial}{\partial \varphi},$$

$$\frac{\partial}{\partial x} = \frac{f}{h_u^2}\left(\sinh u \cos v \frac{\partial}{\partial u} - \cosh u \sin v \frac{\partial}{\partial v}\right),$$

$$\frac{\partial}{\partial x} = \frac{1}{h_\xi^2}\left(\xi \frac{\partial}{\partial \xi} - \eta \frac{\partial}{\partial \eta}\right); \qquad \frac{\partial}{\partial y} = \sin\varphi \frac{\partial}{\partial \rho} + \frac{\cos\varphi}{\rho}\frac{\partial}{\partial \varphi},$$

$$\frac{\partial}{\partial y} = \frac{f}{h_u^2}\left(\cosh u \sin v \frac{\partial}{\partial u} + \sinh u \cos v \frac{\partial}{\partial v}\right),$$

$$\frac{\partial}{\partial y} = \frac{1}{h_\xi^2}\left(\eta \frac{\partial}{\partial \xi} + \xi \frac{\partial}{\partial \eta}\right),$$

from which the operators $\hat{U}^{\pm}$ of (A.12) are found to be

$$\hat{U}^{\pm} \equiv \frac{1}{\sqrt{2}k_t} \exp\left\{\pm \mathrm{i}\varphi\right\}\left(\frac{\partial}{\partial \rho} \pm \mathrm{i}\frac{1}{\rho}\frac{\partial}{\partial \varphi}\right), \tag{B.17}$$

$$\hat{U}^{\pm} = \frac{1}{\sqrt{2}k_t h_u} \exp\left\{\pm \mathrm{i}\alpha\,(u, v)\right\}\left(\frac{\partial}{\partial u} \pm \mathrm{i}\frac{\partial}{\partial v}\right), \tag{B.18}$$

$$\hat{U}^{\pm} \equiv \frac{1}{k_t h_\xi} \exp\left\{\pm \mathrm{i}\beta\,(\xi, \eta)\right\}\left(\frac{\partial}{\partial \xi} \pm \mathrm{i}\frac{\partial}{\partial \eta}\right). \tag{B.19}$$

Consequently, the combinations of unit vectors and transverse derivatives appearing in (A.9)–(A.11), applied to the corresponding representations of (B.14)–(B.19), lead to

$$\hat{\mathbf{e}}^{\pm}\hat{U}^{\mp} = \frac{1}{\sqrt{2}k_t}(\hat{\mathbf{e}}_1 \pm \mathrm{i}\hat{\mathbf{e}}_2)\left(\frac{1}{h_1}\frac{\partial}{\partial q_1} \mp \mathrm{i}\frac{1}{h_2}\frac{\partial}{\partial q_2}\right), \tag{B.20}$$

where the products of the complex conjugate phase factors in equations (B.14)–(B.16) and (B.17)–(B.19) reduce to one.

Finally, an interpretation of the operators $\hat{U}^{\pm}$ can be provided in terms of *ladder operators associated to circular cylindrical symmetry*, since applying them to the scalar Bessel solution $\psi_l(\rho, \varphi) = J_l(k_t\rho)\exp(\mathrm{i}l\varphi)$ gives rise to

$$\hat{U}^{\pm}\psi_l(\rho, \varphi) = \sqrt{2}\mathrm{i}\psi_{l\pm1}(\rho, \varphi).$$

It is important to remark, however, that this is an exclusive feature of the circular symmetry and the associated orbital angular momentum. In other coordinate systems, the same operator is well defined, but its physical or geometrical effects have to be investigated.

References

[1] Durnin J 1987 Exact solutions for non-diffracting beams. I. The scalar theory *J. Opt. Soc. Am.* A **4** 651–4

[2] Durnin J, Miceli J J and Eberly J H 1987 Diffraction-free beams *Phys. Rev. Lett.* **58** 1499–501

[3] Gutiérrez-Vega J C, Iturbe-Castillo M D and Chávez-Cerda S 2000 Alternative formulation for invariant optical fields: Mathieu beams *Opt. Lett.* **25** 1493–5

[4] Gutiérrez-Vega J C, Bandres-Motola M A, Ley-Koo E, Volke-Sepúlveda K and Chávez-Cerda S 2003 Parabolic propagation-invariant optical beams *Conf. Lasers and Electro-Optics/Europe and European Quantum Electronics Conf.: Postdeadline Papers CEP1-5*

[5] Bandres M A, Gutiérrez-Vega J C and Chávez-Cerda S 2004 Parabolic nondiffracting optical wave fields *Opt. Lett.* **29** 44–6

[6] Gori F, Guattari G and Padovani C 1987 Bessel–Gauss beams *Opt. Commun.* **64** 491–5

[7] Li Y, Lee H and Wolf E 2004 New generalized Bessel–Gauss beams *J. Opt. Soc. Am.* A **21** 640–6

[8] Gutiérrez-Vega J C and Bandres M A 2005 Helmholtz–Gauss waves *J. Opt. Soc. Am.* A **22** 289–98

[9] Bouchal Z and Olivik M 1995 Non-diffractive vector Bessel beams *J. Mod. Opt.* **42** 1555–66

[10] Bouchal Z and Olivik M 1997 Non-diffractive stationary electromagnetic field *Opt. Commun.* **133** 315–27

[11] Volke-Sepúlveda K, Garcés-Chávez V, Chávez-Cerda S, Arlt J and Dholakia K 2002 Orbital angular momentum of a high-order Bessel light beam *J. Opt. B: Quantum Semiclass. Opt.* **4** S82–9

[12] Lekner J 2004 Invariants of three types of generalized Bessel beams *J. Opt. A: Pure Appl. Opt.* **6** 837–43

[13] Bandres M A and Gutiérrez-Vega J C 2005 Vector Helmholtz–Gauss and vector Laplace–Gauss beams *Opt. Lett.* **30** 2155–7

[14] Arlt J and Dholakia K 2000 Generation of high-order Bessel beams by use of an axicon *Opt. Commun.* **177** 297–301

[15] Flores-Pérez A, Hernández-Hernández J, Jáuregui R and Volke-Sepúlveda K 2006 Experimental generation and analysis of first-order TE and TM Bessel modes in free space *Opt. Lett.* **31** (11)

[16] Allen L, Beijersbergen M W, Spreeuw R J C and Woerdman J P 1992 Orbital angular momentum of light and the transformation of Laguerre–Gaussian laser modes *Phys. Rev.* A **45** 8185–9

[17] Stratton J A 1941 *Electromagnetic Theory* (New York: McGraw-Hill) pp 392–4

[18] Ley-Koo E and Volke-Sepúlveda K 2006 Geometry and dynamics of scalar propagation invariant Mathieu and parabolic optical fields, in preparation

[19] Born M and Wolf E 1999 *Principles of Optics* 7th (expanded) edn (Cambridge: Cambridge University Press) pp 30–31

[20] Gutiérrez-Vega J C, Rodriguez-Dagnino R M and Chávez-Cerda S 2002 Attenuation characteristics in confocal annular elliptic waveguides and resonators *IEEE Trans. Microw. Theory Tech.* **50** 1095–100

[21] Turunen J and Friberg A T 1993 Self-imaging and propagation-invariance in electromagnetic fields *Pure Appl. Opt.* **2** 51–60

[22] Garcés-Chávez V, McGloin D, Padgett M J, Dultz W, Schmitzer H and Dholakia K 2003 Observation of the transfer of the local angular momentum density of a multi-ringed light beam to an optically trapped particle *Phys. Rev. Lett.* **91** 093602

[23] Chávez-Cerda S, Gutiérrez-Vega J C and New G H C 2001 Elliptic vortices of electromagnetic wavefields *Opt. Lett.* **26** 1803–5

[24] López-Mariscal C, Gutiérrez-Vega J C, Milne G and Dholakia K 2006 Orbital angular momentum transfer in helical Mathieu beams *Opt. Express* **14** 4183–8

[25] Chávez-Cerda S, New G H C, Gutiérrez-Vega J C, Allison I, O'Neil A T, MacVicar I, Padgett M J and Courtial J 2002 Holographic generation and orbital angular momentum of high-order Mathieu beams *J. Opt. B: Quantum Semiclass. Opt.* **4** S52–7

[26] Jackson J D 1998 *Classical Electrodynamics* 3rd edn (New York: Wiley) p 608

[27] Lekner J 2003 Polarization of tightly focused laser beams *J. Opt. A: Pure Appl. Opt.* **5** 6–14

[28] Lekner J 2004 Invariants of electromagnetic beams *J. Opt. A: Pure Appl. Opt.* **6** 204–9

[29] Arfken G B and Weber H J 1995 *Mathematical Methods for Physicists* 4th edn (London: Academic) pp 99–118